From Ameen, M. S. (ed.), 1995, *Fractography: fracture topography as a tool in fracture mechanics and stress analysis*
Geological Society Special Publication No. 92, pp. 215–233

Factors controlling joint spacing in interbedded sedimentary rocks: integrating numerical models with field observations from the Monterey Formation, USA

MICHAEL R. GROSS,[1] MARK P. FISCHER,[2] TERRY ENGELDER[2] & ROY J. GREENFIELD[2]

[1]*Department of Geology, Florida International University, Miami, FL 33199, USA*

[2]*Department of Geosciences, Pennsylvania State University, University Park, PA 16802, USA*

Abstract: Local tensile stress normal to a joint is reduced in the vicinity of the joint because such stresses are not transmitted across free surfaces. This stress reduction prevents the formation of new joints in the vicinity of existing joints, and thus influences joint spacing. Lateral extent of this stress reduction shadow increases with joint height, which corresponds to bed thickness for many sedimentary rocks. The linear correlation between joint spacing and bed thickness commonly observed in outcrop is a direct result of this relationship. However, other factors in addition to bed thickness influence joint spacing. We evaluate these factors through both a review of the Hobbs model for joint spacing and a 2D finite element simulation of a crack confined to a lithology-controlled mechanical unit. The stress reduction shadow increases in length with increasing Young's modulus of the jointing bed, though fracture stress, flaw size, flaw distribution and extensional strain all interact with bed thickness and elastic properties ultimately to control joint spacing. One explanation for the observed decrease in joint spacing with increasing Young's modulus in outcrops of the Monterey Formation is that beds with higher Young's moduli fail at lower magnitudes of extensional strain.

In a 1967 issue of *Geological Magazine*, D. W. Hobbs published a paper entitled 'The formation of tension joints in sedimentary rocks: an explanation', which is commonly cited as a theoretical explanation for joint spacing in rock masses composed of layers, each with a different set of elastic properties. Based on the original derivation of Cox (1952), the Hobbs model provides one theoretical basis for the well-documented linear relationship between joint spacing and bed thickness in sedimentary rocks (e.g. Price 1966; McQuillan 1973; Ladeira & Price 1981; Huang & Angelier 1989; Narr & Suppe 1991; Gross 1993*a*). By relating joint spacing to the Young's modulus of the jointing bed and shear modulus of the bounding non-jointing beds, Hobbs implies that joint spacing is influenced by the elastic properties of each bed.

Though both ingenious and remarkably accurate in its prediction of stress distribution, the Hobbs paper is often misunderstood because it is compact and lacks illustrations. We present a brief explanation of Hobbs' analysis in an effort to clarify the assumptions and implications of his model. In addition, we use a 2D finite element numerical simulation of a crack confined within a bed to describe the stress and displacement fields around the profile section of a crack in an interbedded sedimentary rock mass. Results of the finite element modelling are compared with predictions of the Hobbs model. Finally, we discuss

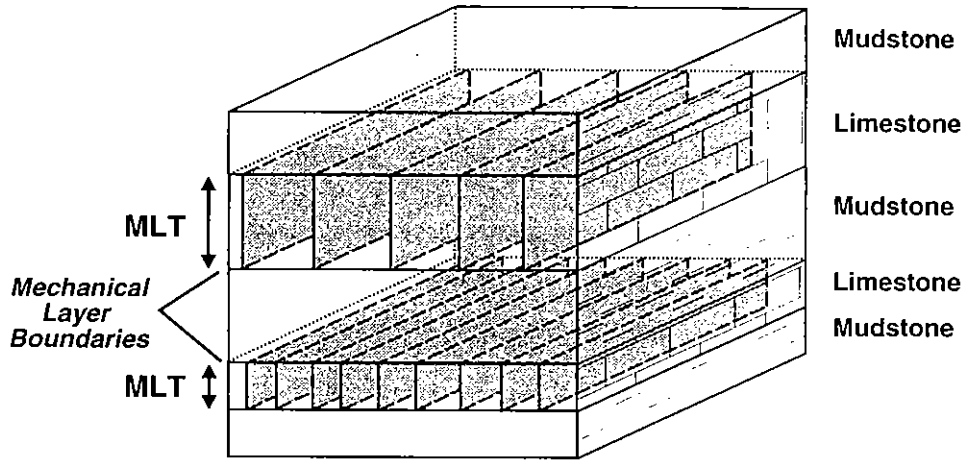

Fig. 1. Sketch of a lithology-controlled mechanical unit, with systematic joints confined to discrete beds, and lithologic contacts serving as mechanical layer boundaries. Note that joint height equals mechanical layer thickness (MLT), and is proportional to joint spacing (from Gross 1993*a*).

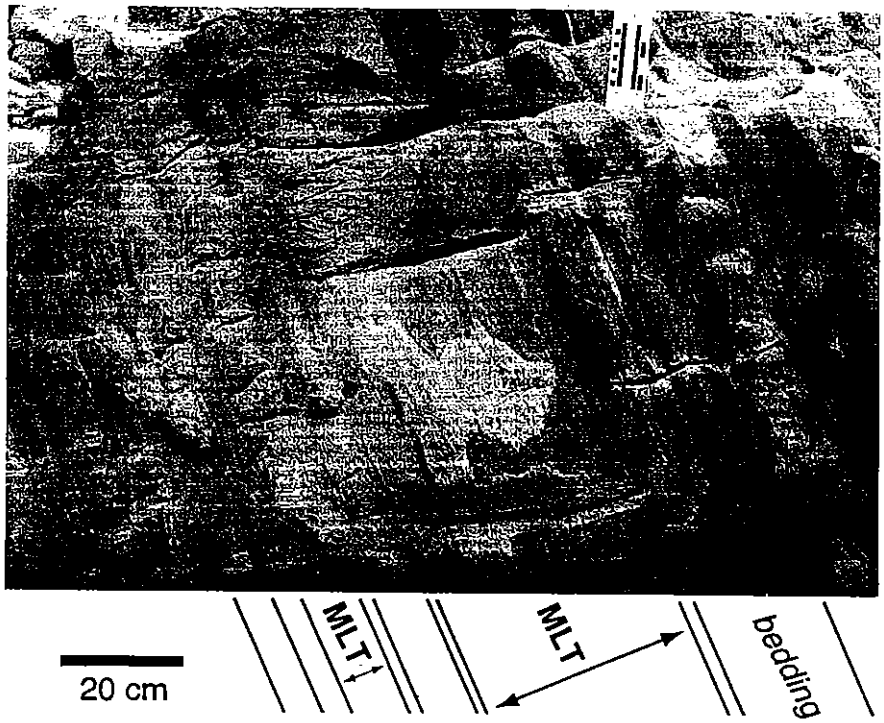

Fig. 2. Photograph of steeply dipping limestone beds in the Monterey Formation exposed at Lion's Head along the Santa Maria coastline of California, demonstrating the relationship between joint spacing and bed thickness. Tall joints, in thicker beds, are more widely spaced than short joints, in thinner beds. Note the consistent joint height for each individual mechanical layer.

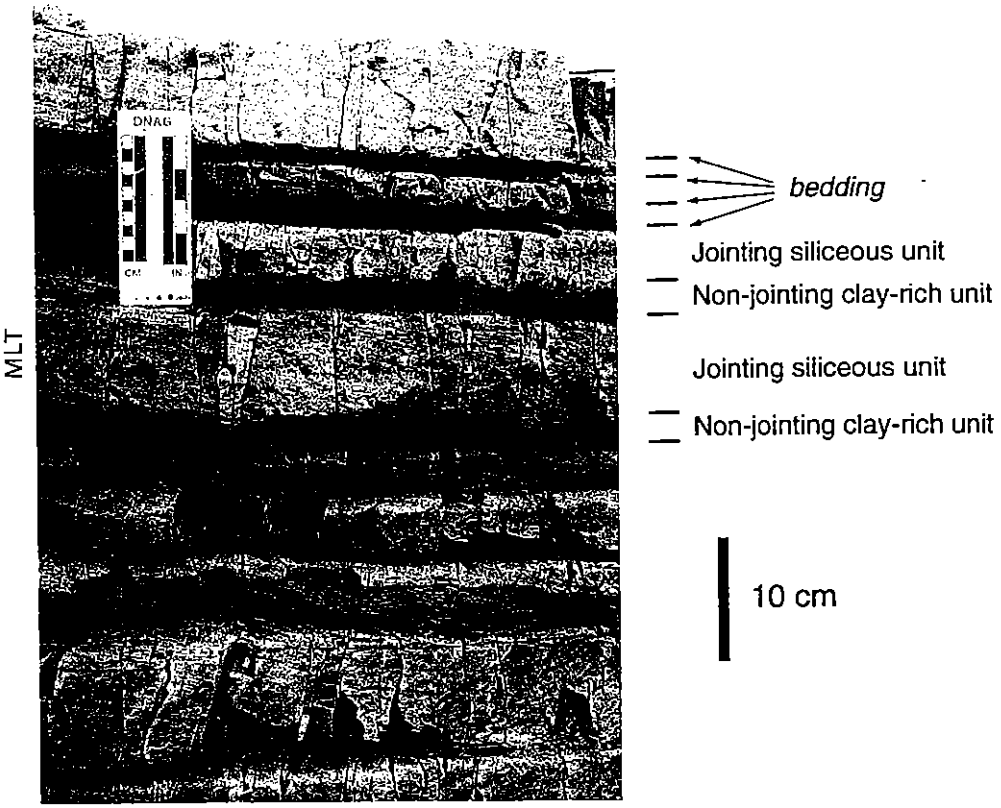

Fig. 3. Photograph of interbedded siliceous (jointing) and mudstone (non-jointing) layers in the Monterey Formation exposed at Purisima Point along the Santa Maria coastline. The light coloured siliceous layers contain statistically regularly-spaced joints that terminate at contacts with adjacent mudstone layers.

the major factors controlling joint spacing and attempt to reconcile these factors with field observations that some stiffer beds in the Monterey Formation of California have more closely spaced joints than beds with lower Young's moduli.

Stress reduction near joints

Joint spacing models for rocks commonly focus on an analysis of stress reduction in the vicinity of joints because the criterion for joint propagation is a threshold stress value, derived either from the tensile strength test (e.g. Jaeger & Cook 1976) or a measure of fracture toughness (e.g. Irwin 1957) of the rock bed. The mechanism for stress build up in these models is layer-parallel stretching, which can occur locally in the extensional region of a fold or regionally upon uplift and erosion.

Stress perturbations occur in the vicinity of an open joint because the joint is a free surface, and hence acts as a barrier to the transmission of tensile stress. Consequently,

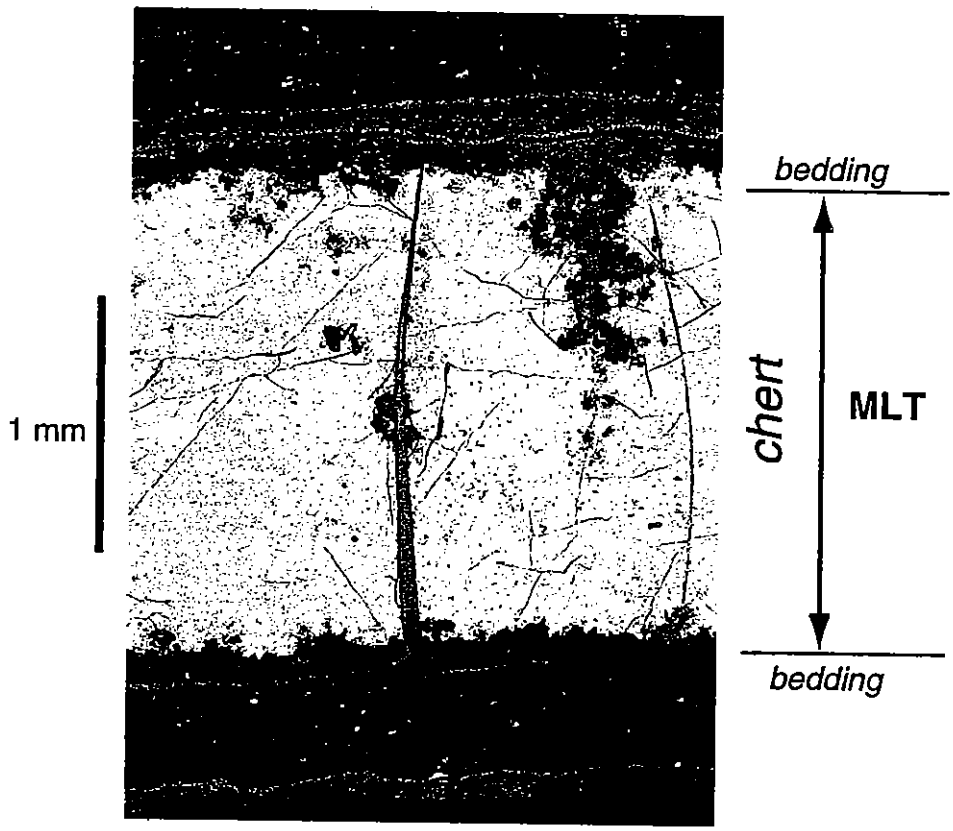

Fig. 4. Photomicrograph of a thin section from core taken from Point Arguello Oilfield, offshore Santa Maria Basin, showing a tensile fracture confined to a quartz chert layer. See text for details.

local crack-normal tensile stress at the joint surface is zero, and increases to the level of far-field tensile stress at an infinite distance from the joint. New joints form where the local tensile stress exceeds the fracture stress of the rock. Thus, models for joint spacing commonly predict the location, and hence spacing, of new joints by evaluating the ratio of local tensile stress to remote tensile stress as a function of distance from the stress-free joint (e.g. Lachenbruch 1961; Pollard & Segall 1987).

Bed thickness – joint spacing relationship and sequential infilling

Joints in sedimentary rocks generally fall into two categories, those that terminate randomly within the rock mass and those that terminate at discrete mechanical layer boundaries. Lithologic contacts, as well as pre-existing fractures, can serve as mechanical layer boundaries, thereby dividing the rock mass into discrete mechanical units (Gross 1993*a*). The analysis presented in this study focuses on joints confined to individual lithologic beds, which are frequently observed in thin to medium bedded sedimentary

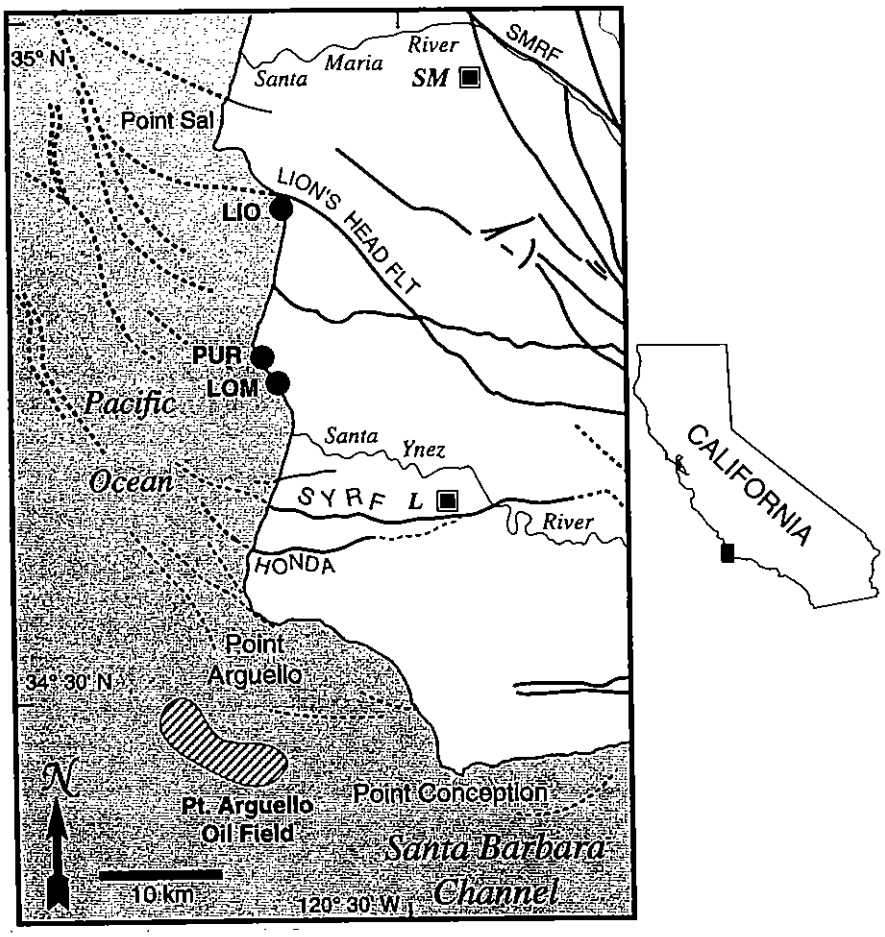

Fig. 5. Location map of the southern Santa Maria coastline showing outcrops where fracture data were collected along with the photographs from Figs 2–4 (adapted from Sylvester & Darrow 1979). Sites include Lion's Head (LIO), Purisima Point (PUR) and Lompoc Landing (LOM). Towns are Santa Maria (SM) and Lompoc (L). SYRF refers to the Santa Ynez River Fault.

sequences (i.e. beds ranging in thickness from *c.* 1 to 100 cm) composed of diverse rock types. In such lithology-controlled mechanical units joints extend from the bottom of the bed to its top so that joint height equals bed thickness, which in turn is proportional to joint spacing, measured as the orthogonal distance between adjacent parallel joints of a particular set (Fig. 1). These relationships are demonstrated in the photographs in Figs 2–4, taken from the Monterey Formation along the central California coastline (Fig. 5). In the interbedded limestone and shale of Fig. 2, joint height in each mechanical layer is uniform, and tall joints are more widely spaced than short joints. The outcrop shown in Fig. 3 consists of a series of well-defined jointing and non-jointing lithologies, in which joints are confined solely to the light coloured siliceous layers and display a regular spacing. In contrast, the thin recessive shaley layers act as mechanical layer boundaries and remain unjointed. An example of a joint confined to a thin quartz chert layer is shown

in Fig. 4. Note the joint terminates abruptly at the contact with adjacent shale layers. Although slip has occurred in the immediate vicinity of the crack, in general the widest contact does not serve as a detachment.

Though numerous statistical functions, ranging from negative exponential to normal, have been proposed to describe the general distribution of joint spacing (e.g. Priest & Hudson 1976; Rouleau & Gale 1985; Rives *et al.* 1992), the specific case of lithology-controlled joints leads to a typically skewed log normal or gamma distribution for joints belonging to an individual systematic set (e.g. Huang & Angelier 1989; Narr & Suppe 1991). The regular spacing may be due to the stress reduction shadow created by pre-existing joints (e.g. Hobbs 1967) and the sequential joint infilling process, whereby new joints form in a sequential fashion between adjacent pre-existing joints (Gross 1993*a*). The non-normal distribution may result from the random distribution of flaws, which serve as initiation points for joints. While other studies focus on interactive joint growth (e.g. Pollard *et al.* 1982; Olson & Pollard 1989), we are concerned with identifying where new joints will form with respect to pre-existing joints along the profile section of a layer. Therefore, throughout this paper we consider the actual joint propagation process as instantaneous relative to the time between sequential infilling stages of a systematic joint set.

Material science studies provide evidence in favour of a sequential infilling mechanism for joints confined to lithology-controlled mechanical layers. Tension tests performed on layered ceramics demonstrate that in addition to an increase in crack spacing with layer thickness, average crack spacing decreases systematically with increasing applied stress (Garrett & Bailey 1977; Parvizi & Bailey 1978). The applied stress in turn scales linearly with extensional strain for the elastic laminates. The decrease in crack spacing with increasing load occurs by a process of sequential infilling. Geological evidence supporting sequential infilling includes fractured piedmontite grains (Masuda & Kuriyama 1988) and curving cross joints (Engelder & Gross 1993).

The Hobbs model for joint spacing

The 1D Hobbs model consists of three discrete beds and predicts variations in the crack-normal tensile stress as a function of differences in elastic properties between a middle jointing bed and two non-jointing bounding beds. The beds behave elastically and are bonded together to prevent slip along the interfaces. Unlike the non-layered models of Lachenbruch (1961) and Pollard & Segall (1987), stress perturbations in a bedded medium are influenced by both elastic properties and shear stresses that develop along bed interfaces. According to our interpretation, the Hobbs model consists of a middle 'jointing bed' (Bed A) sandwiched between 'non-jointing beds' (Beds B). Hobbs assumes both bounding beds have the same elastic moduli, and that the thickness of bounding beds is much greater than the thickness (d) of the jointed bed. After initial extension all of the beds remain unjointed, however, as extensional strain increases, the tensile stress in the middle bed eventually exceeds the tensile strength of that bed, and a joint propagates. At this point Hobbs assumes that tensile stress cannot be transmitted across the joint surface. Shear stresses are produced within the bounding beds as a direct result of differences in elastic displacement within the jointed bed and bounding beds.

The key parameter controlling joint spacing is the distribution of longitudinal tensile stress (σ_{xx}) within Bed A after jointing, which increases from zero at the joint surface to a value equivalent to the remote stress at an infinite distance away from the joint.

Substituting Hobbs' equation 13 into equation 6 and rearranging the terms produces an equation that evaluates normalized crack-normal tensile stress after joint propagation (i.e. local stress divided by remote tensile stress) as a function of distance from the joint;

$$\frac{P}{E_A d\epsilon_1} = \frac{\sigma_{local}}{\sigma_{remote}} = 1 + \sinh\frac{2x}{d}\left(\frac{G_B}{E_A}\right)^{\frac{1}{2}} - \cosh\frac{2x}{d}\left(\frac{G_B}{E_A}\right)^{\frac{1}{2}}, \quad (1)$$

where P is the applied load, ϵ_1 is the strain at which the first joint forms, d is the jointing bed thickness (i.e. joint height), and E_A and G_B are the Young's modulus and shear modulus of the jointing and non-jointing beds, respectively. We prefer to rewrite equation (1) in the form:

$$\frac{P}{E_A d\epsilon_1} = f(x/\delta), \quad (2)$$

where,

$$\delta = \frac{d}{2}\left(\frac{E_A}{G_B}\right)^{\frac{1}{2}}, \quad (3)$$

and $f(x/\delta)$ gives the dependence of the local stress on x. The function $f(x/\delta)$ is 0 for $x=0$ and increases to 1 for large x. The quantity δ has units of length and can be thought of as a decay length, or the distance over which the stress shadow decays back to a fixed fraction of the remote stress. The distance δ is proportional to d and to the square roof of (E_A/G_B).

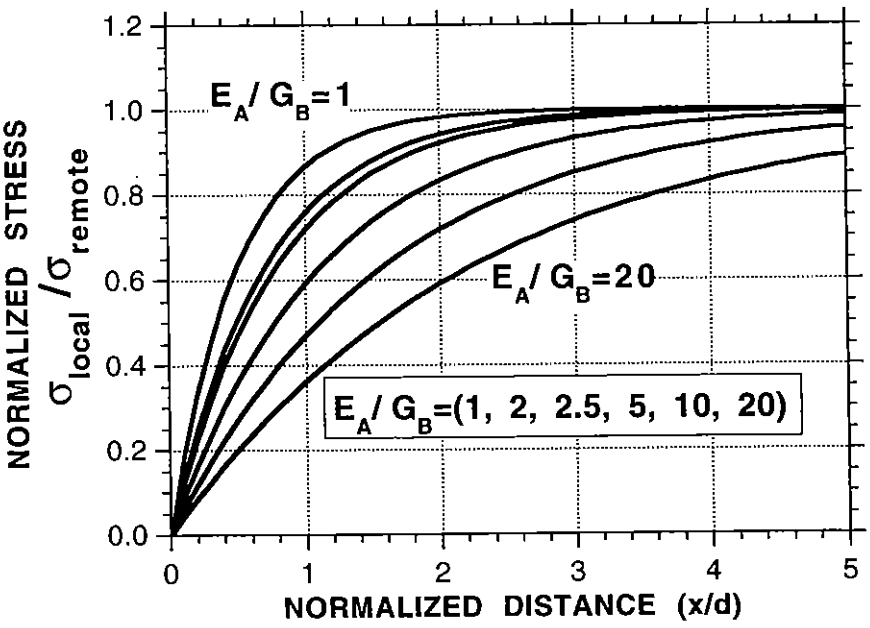

Fig. 6. Predicted plots of stress reduction shadows based on the Hobbs model for various E_A/G_B ratios.

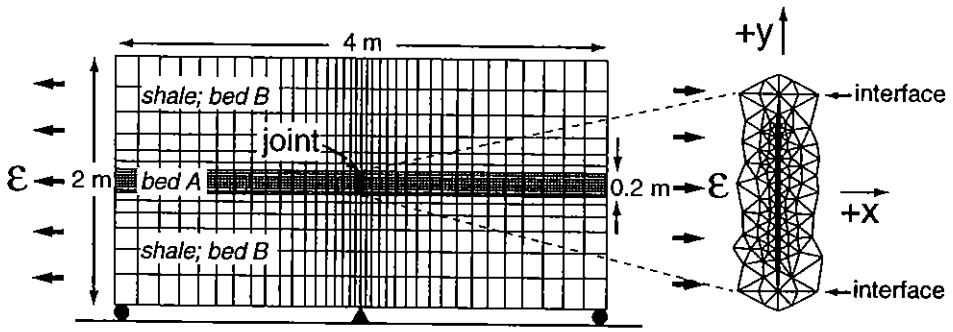

Fig. 7. Finite element mesh and boundary conditions. Models were subjected to uniform longitudinal extension, ϵ. Inset shows an enlarged portion of mesh around joint in Bed A. Bed B is shale in all models whereas the material properties of Bed A are varied. Joint shown slightly open for illustration. Cartesian coordinate system with (0, 0) at the centre of the joint is used for all related graphs and figures (after Fischer 1994).

A plot of normalized stress v. normalized distance from a joint for a series of E_A/G_B ratios is presented in Fig. 6. Because Hobbs' analysis predicts that for a fixed shear modulus of the bounding beds (i.e. holding G_B constant), δ will increase as the square root of E_A, a high E_A will produce a long stress reduction shadow, whereas a low E_A creates a short perturbed zone.

Table 1. *Boundary conditions and elastic properties assigned to finite element models*

Model #	ϵ_{xx}	E_B (GPa)	E_A (GPa)	ν_B	ν_A	G_B (GPa)	G_A (GPa)
1	5×10^{-4}	16	56	0.14	0.26	7	22
2	5×10^{-4}	16	17.5	0.14	0.25	7	7
3	5×10^{-4}	16	35	0.14	0.25	7	14
4	5×10^{-4}	16	70	0.14	0.25	7	28

Finite element modelling

We conducted a series of 2D finite element models to determine the distribution of stresses and displacements in a jointed, interbedded rock body, and to investigate the effects of contrasting elastic moduli on stress perturbations near joints. Finite element numerical simulation was accomplished using the interactive fracture analysis program FRANC (Wawrzynek & Ingraffea 1987). FRANC simulates the $r^{-1/2}$ singularity in the elastic crack-tip stress field by surrounding each crack tip with a rosette of eight quadratic, triangular, isoparametric quarter-point elements (Barsoum 1976); the remainder of the model mesh is composed of quadratic, isoparametric elements. The boundary conditions and geometry of the model are shown in Fig. 7. Model material properties (Table 1) are median values compiled from several published sources (Blair 1955, 1956; Clark 1966; Senseny & Pfeifle 1984; Atkinson & Meridith 1987).

In the first model, the 2D distribution of crack-normal tensile stress (σ_{xx}) was analysed in detail for a model consisting of a dolostone bed (Bed A; $E = 56$ GPa; $G = 22$ GPa;

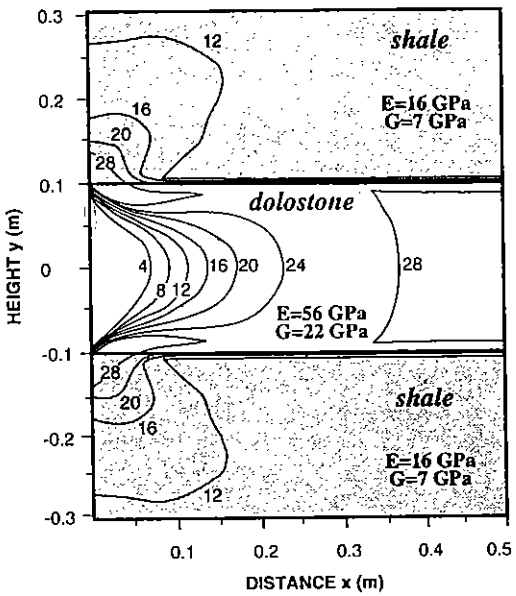

Fig. 8. Contour diagram showing the 2D distribution of crack-normal tensile stress (σ_{xx}) in MPa for a portion of the dolostone and shale model to the right of the joint. Model subjected to a strain of 5×10^{-4} (after Fischer 1994).

$\nu = 0.26$) bounded by shale beds (Bed B; $E = 16$ GPa; $G = 7$ GPa; $\nu = 0.14$). A uniform longitudinal extensional strain of 5×10^{-4} was applied, resulting in theoretical pre-cracking stresses of 28 MPa in the dolostone and 8 MPa in the shale beds. Because of edge effects in the finite element model, however, σ_{xx} varied longitudinally within each bed prior to cracking. This variation was minor (< 2.0% mean error in each bed), and in the model the mean σ_{xx} is 28.5 MPa in dolostone and 7.8 MPa in shale.

Local crack-normal tensile stress

Local crack-normal tensile stress (σ_{xx}) in the dolostone is reduced near the joint whereas in the shale there is an increase in σ_{xx} near the joint (Fig. 8). At the joint wall σ_{xx} is zero and near each end of the joint the stress is elevated due to the stress concentrating effect of the sharp crack tip (Lawn & Wilshaw 1975; Broek 1978). Because the joint is elliptical, the greatest amount of elastic strain (and hence stress) is relieved by crack opening along the middle of Bed A. Consequently, the stress reduction is greatest and extends farthest along the centre of Bed A. This combination of elliptical crack shape, high stress near the joint tip and zero stress along the length of the joint is responsible for the concave-inwards shape of the stress reduction shadow in the dolostone bed. Because there is no crack opening in the shale beds, large elastic strains developed in shale adjacent to the joint tips result in a localized increase in stress. An integral part of linear elastic fracture mechanics (Irwin 1957; Paris & Sih 1965; Broek 1978), this stress concentration is maximum at the joint tips and decreases rapidly away from the joint. At horizontal distances > 0.3 m from the joint the stress in the shale beds is the same as the pre-cracking stress.

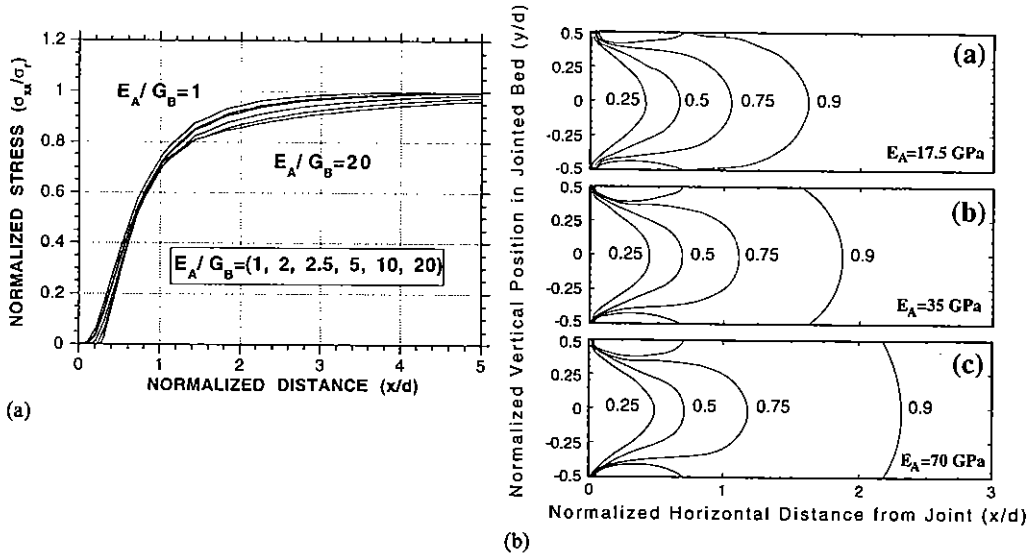

Fig. 9 (**a**) Graph of normalized σ_{xx} v. normalized horizontal distance from the joint for various E_A/G_B values calculated using FRANC. G_B for all models is 7 GPa. Stress values were recorded along centre of Bed A. (**b**) Contours of normalized σ_{xx} in a middle bed of $\nu = 0.25$ and variable E_A. Bounding beds are shale in all three models and E_A/G_B ratios are 2.5, 5 and 10 in (a), (b) and (c), respectively. Contours are in percentages of the pre-cracking stress in each layer (i.e. a value of 0.5 indicates the stress at that position is 50% of the pre-cracking stress value) (after Fischer 1994).

Elastic moduli effects

In order to investigate the effects of varying elastic moduli (i.e. E_A/G_B ratios) on joint spacing we conducted a series of models in which a bed with $\nu = 0.25$ and variable E_A is sandwiched between shale beds and subjected to a uniform longitudinal extensional strain of 5×10^{-5}. The ratio of E_A/G_B controls the lateral extent of the stress reduction shadow around a joint, as shown graphically in Fig. 9a. To illustrate this effect better, Fig. 9b shows contours of normalized stress in the middle bed for three geologically reasonable values of E_A/G_B. For values of normalized $\sigma_{xx} < 0.75$, the stress reduction shadows for various E_A/G_B ratios are nearly identical. However, for values of normalized stress > 0.75 the size of the stress reduction shadow increases significantly with increasing E_A.

Comparison with Hobbs' analysis

In general there is good agreement between Hobbs' analysis and our finite element model results. Although Hobbs' prediction of the dependence of stress reduction shadow size on contrasts in elastic moduli is in qualitative agreement with the finite element model results (i.e. the stress shadow increases in extent with increasing Young's modulus), the dependence of the stress shadow decay length, d, on E_A exhibited by FRANC is weaker than the square root dependence predicted by the Hobbs model. To show this we consider the x position of the finite element contours of normalized σ_{xx} at the centre of Bed A,

denoted by $x^{(m)}$ (Fig. 9b). These positions are compared to those predicted by the Hobbs model, denoted by $x^{(p)}$. The $x^{(p)}$ values for each contour are computed as:

$$x^{(p)}_{(E_A)} = x^{(m)}_{(17.5)}\sqrt{\frac{E_A}{17.5}}, \tag{4}$$

and are given in Table 2. This definition of $x^{(p)}$ gives Hobbs' prediction of the x position of each contour for the case in which E_A is 35 and 70 GPa (i.e. $x^{(p)}_{(35)}$, $x^{(p)}_{(70)}$) based on the position of the corresponding contour for the finite element model in which E_A is 17.5 GPa (i.e. $x^{(m)}_{(17.5)}$). The $x^{(p)}$ values calculated for the models in which E_A is 35 and 70 GPa are in all cases greater than the corresponding $x^{(m)}$ values, showing that dependence of the stress reduction shadow size on E_A is weaker for the finite element model than the square root dependence predicted by Hobbs.

Model geometry and method of stress determination may contribute in part to the differences in stress reduction shadow size predicted by the Hobbs and finite element models. In the finite element model the joint terminates at the shale boundaries and is entirely confined to the middle layer, thus reflecting geometry commonly observed in interbedded rocks with sharp lithologic contacts (Figs 3 & 4). In contrast, the joint in the Hobbs model extends significant distances into the neighbouring beds due to requirements imposed by shear stress assumptions. Furthermore, as opposed to Hobbs' derivation, the numerical model utilizes linear elastic fracture mechanics to describe the stress and displacement fields in the vicinity of the crack.

Table 2. *Comparison of finite element stress reduction contours to the* $(E_A/G_B)^{1/2}$ *dependence predicted by the Hobbs model*

	Contour level							
	0.25		0.50		0.75		0.90	
E_A (GPa)	$x^{(m)}$	$x^{(p)}$	$x^{(m)}$	$x^{(p)}$	$x^{(m)}$	$x^{(p)}$	$x^{(m)}$	$x^{(p)}$
17.5	0.403	0.403	0.655	0.655	1.042	1.042	1.613	1.613
35	0.420	0.570	0.682	0.927	1.075	1.473	1.848	2.281
70	0.470	0.806	0.706	1.310	1.176	2.083	2.318	3.226

In all models G_B is 7 GPa and distances are normalized to a bed thickness of 1. $x^{(m)}$ refers to the contour position in the numerical model and $x^{(p)}$ is the position predicted by Hobbs.

Joint spacing predicted from numerical models

Joint spacing models combine a rock fracture criterion with an analysis of the stress distribution around a pre-existing joint to predict the location where subsequent joints will form (e.g. Hobbs 1967; Pollard & Segall 1987; Narr & Suppe 1991; Gross 1993*a*). Hobbs employs a tensile strength fracture criterion wherein joints form when the remote tensile stress (σ_{remote}) in a bed exceeds the tensile strength. We use a fracture criterion based on the principles of linear elastic fracture mechanics (Lawn & Wilshaw 1975).

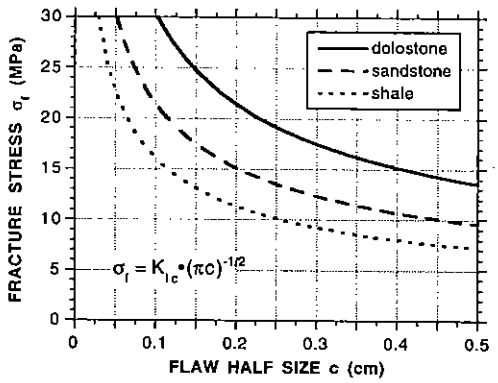

Fig. 10. Flaw size dependent fracture criterion. Fracture stress for dolostone, sandstone and shale illustrated for various flaw sizes. Fracture toughness values for sandstone (K_{Ic} = 1.2 MPa m$^{1/2}$), shale (K_{Ic} = 0.9 MPa m$^{1/2}$) and dolostone (K_{Ic} = 1.7 MPa m$^{1/2}$) are the mean of K_{Ic} values compiled in the literature (Senseny & Pfeifle 1984; Atkinson & Meredith 1987).

Fracture criterion

Inglis (1913) and Griffith (1920) showed that brittle fracture is often induced by a tensile stress concentration at flaws (e.g. microcracks) in a material. Linear elastic fracture mechanics describes the stress concentration at the tip of a Mode I opening (i.e. tensile) crack by means of the stress intensity factor (Broek 1978):

$$K_I = Y\sigma_{remote}\sqrt{\pi c}, \tag{5}$$

where σ_{remote} is the remote crack-normal tensile stress, c is half the crack length, and Y is a geometric constant, commonly taken as 1.0 for an infinite flat blade crack (Lawn & Wilshaw 1975). The fracture criterion states that a crack will propagate when stress intensity at the crack tip exceeds some critical value known as the fracture toughness (K_{Ic}) of the material (Irwin 1957). Substituting K_{Ic} for K_I in equation (5), setting $Y = 1$, and solving for the fracture stress (σ_f), the crack-normal tensile stress required to cause a flaw to propagate, it is found that:

$$\sigma_f = \frac{K_{Ic}}{\sqrt{\pi c}}. \tag{6}$$

Using published values of K_{Ic} for a variety of rock types, σ_f can be calculated for a given flaw size (Fig. 10). However, because the distribution of flaw sizes in rocks is complex, it is unlikely that the fracture strength of a rock can be defined by a single value of σ_f.

Flaw size distribution in two dimensions

The remote tensile stress required to drive a crack decreases with initial flaw size (Fig. 10). As a consequence, for a constant applied extensional strain, the minimum allowable distance between two adjacent joints decreases with increasing flaw size. The dependence

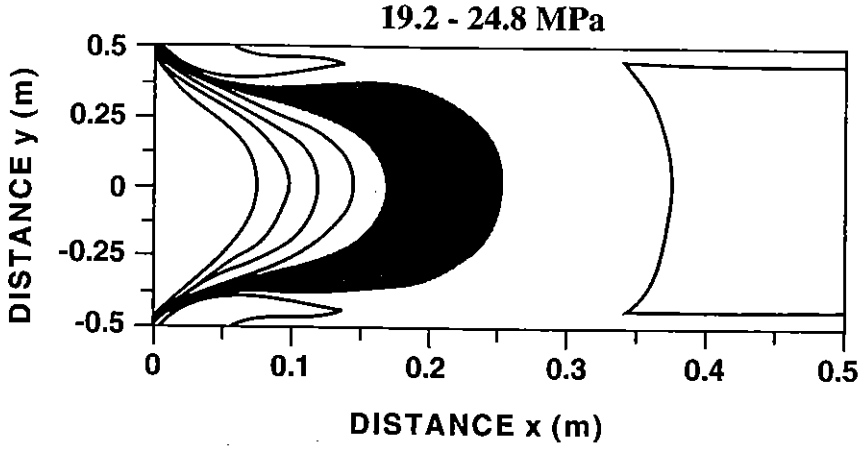

Fig. 11. Stress reduction shadow in the dolostone bed of the dolostone and shale model. Tensile stress contours are in MPa, and applied remote stress is 28.5 MPa. The closest distance at which a new joint will form is dependent on the size of the flaw from which it initiates. Flaws ranging in size from 0.3 to 0.5 cm will activate in the shaded region, with 0.5 cm flaws initiating closer to the joint. Joint spacing therefore decreases with increasing initial flaw size.

of joint spacing on flaw size is shown schematically in Fig. 11, which displays stress contours around a joint in the model dolostone bed (extensional strain of 5×10^{-4}; applied remote stress of 28.5 MPa). As flaw size increases, the corresponding fracture stress at which point the flaw grows into a joint is attained at distances closer to an existing joint, resulting in a decrease in joint spacing. Joint propagation occurs in the shaded region of Fig. 11 for flaws ranging in size from 0.3 to 0.5 cm. In the case of joints initiating in the middle of the bed (i.e. $y = 0$) the minimum allowable joint spacing ranges from $(0.82)d$ for 0.5 cm flaws to $(1.25)d$ for 0.3 cm flaws, where d is the bed thickness.

In addition to flaw size distribution along the x-axis, another factor that determines joint spacing is the position relative to the bed boundary (i.e. along the y-axis) from where the joint initiates. Contour shapes in Fig. 11 predict that for a given flaw size, joints initiating near bed boundaries will be more closely spaced than joints propagating from the central region of beds. The curvature of stress contours is less pronounced for large distances from the joint, so that for the 90% contour level the dependence of joint spacing on y-axis-initiation position is somewhat reduced. Furthermore, a Weibull approach to the strength of materials (e.g. Weibull 1951; Davidge 1979) implies that joint initiation is more likely to occur near the centre of the bed rather than along its edges. This is due to the greater activation area in the central portion of the bed as indicated by the width of the shaded zone in Fig. 11.

Joint spacing determination

Several approaches have been proposed for analysing joint spacing in 1D models, including the maximum tensile stress criterion that predicts precise midpoint fracturing regardless of initial joint spacing (Hobbs 1967), the introduction of random flaws into stress reduction models (Narr & Suppe 1991; Rives *et al.* 1992), and the minimum

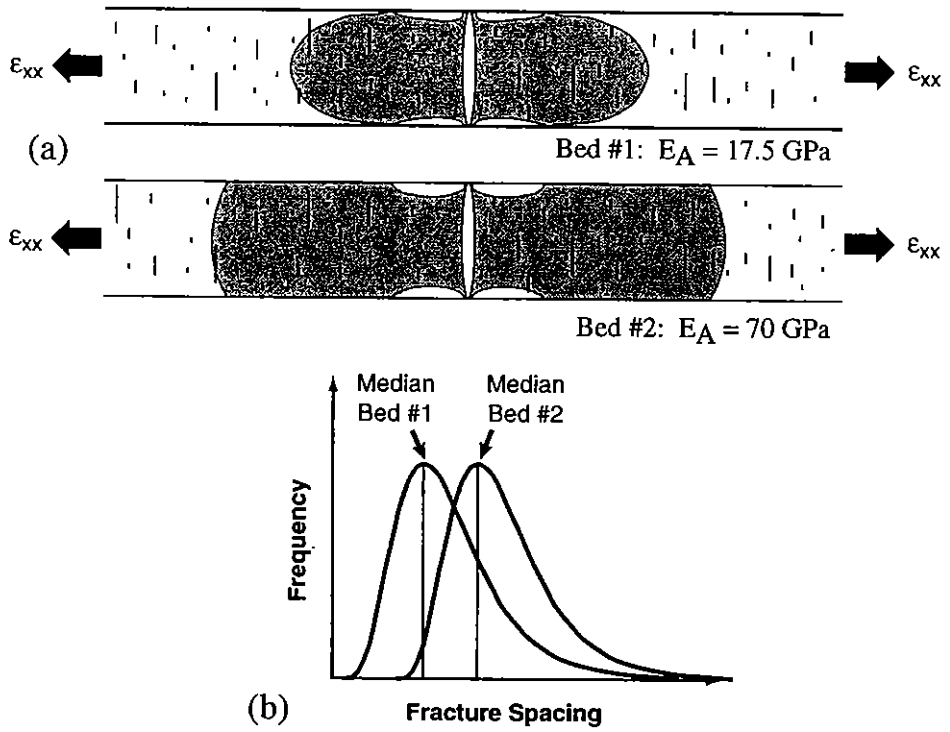

Fig. 12. (**a**) Stress shadows representing 90% of the remote tensile stress for beds with Young's modulus of 17.5 GPa (Bed #1) and 70 GPa (Bed #2). (**b**) Expected joint spacing distributions for Beds #1 and #2 after an equal number of infilling events. Note the larger stress reduction shadow leads to a larger median joint spacing.

allowable spacing criterion (Gross 1993*a*). Regardless of the approach, two boundary conditions always apply to models of joint spacing in lighology-controlled mechanical layers. First, a new joint will form between two pre-existing joints when the fracture stress is attained. Second, the stress reduction shadow inhibits the formation of new joints in the vicinity of pre-existing joints.

Our numerical results from 2D models indicate that the extent of the stress reduction shadow increases with increasing Young's modulus. The effect of elastic properties on joint spacing is illustrated in an example of two jointing layers, #1 and #2, with Young's moduli of 17.5 and 70 GPa, respectively (Fig. 12a). Consider the case whereby each bed has undergone an initial fracturing episode. A subsequent infilling event will result in the joint spacing distributions depicted in Fig. 12b. Random flaw distributions along with the 2D shape of the activation zone will lead to a wide range of joint spacing values and a characteristic skewed distribution. For example, joints will initiate preferentially from the largest flaws, and joints initiating near bed boundaries will be more closely spaced than joints propagating from the central portion of the bed. Nevertheless, one would initially predict that for a population of mechanically confined fractures, the bed with the higher Young's modulus will exhibit a larger median joint spacing because of the larger stress reduction shadow.

Table 3. *Fracture spacing measurements at Lompoc Landing along with physical properties of siliceous mechanical units in the Monterey Formation*

	Chert	Diatomite
Number of beds	6	7
Number of joint spacings	247	315
Matrix porosity	0.5%	37%
Young's modulus	70 GPa	5 GPa
Shear modulus	33 GPa	2 GPa
Fracture spacing index (FSI)	2.41	1.09
Fracture spacing ratio (FSR)	2.29	1.11

Porosity and elastic moduli measurements are preliminary and were determined from similar units exposed along the Santa Maria coastline. Elastic properties were measured dynamically using the resonance technique. From Gross 1993*b*.

Why stiffer beds have smaller joint spacings; a field example from the Monterey Formation, California

The concept that differences in elastic properties among jointing lithologies will result in different joint spacings for a given bed thickness is intuitive. Our analysis thus far suggests the stress shadow increases in lateral extent with increasing Young's modulus, implying that joint spacing should be greater in beds with higher Young's moduli (i.e. stiffer beds) (Fig. 9b). However, joint spacing is often closer in stiffer beds. For example, the siliceous Monterey Formation exposed at Lompoc Landing along the Santa Maria coastline of California (Fig. 5) consists of a series of interbedded cherts and dolomitic diatomites, both jointing lithologies, along with non-jointing clay-rich mudstones. Typical physical properties of the two siliceous rock types, exposed along the Santa Maria coastline, are markedly different from each other, with a Young's modulus of 70 GPa for the quartz chert and 5 GPa for the impure diatomite (Table 3). Several beds at Lompoc Landing are welded together along their boundaries, and consequently were subjected to equal amounts of extensional strain. The vertical systematic joint set investigated trends NNE–SSW and post-dates silica diagenesis, and therefore developed after differences in physical properties were established among the mechanical units.

Joint spacing data for the diatomite and chert beds at Lompoc Landing are presented as plots of median joint spacing v. mechanical layer thickness (Fig. 13). The slope of the best-fit line, calculated with median joint spacing as the dependent variable, is defined as the fracture spacing index (FSI) of Narr & Suppe (1991). The fracture spacing ratio (FSR) equals the mechanical layer thickness divided by the median joint spacing, and represents the mean for all beds of a given lithology. Chert beds at Lompoc Landing display significantly higher FSI and FSR, and thus more closely spaced joints relative to bed thickness, than adjacent diatomites. This spacing relationship exists despite the much larger chert Young's modulus. How does such a joint spacing distribution develop in light of the numerical models and theoretical considerations discussed in this paper? One explanation is that despite the larger stress reduction shadow, a stiffer bed will contain more joints relative to other beds because jointing in the stiffer bed occurs at lower strain levels.

Consider a rock mass composed of a sequence of dolostone and sandstone beds interbedded with non-jointing mudstone beds. The dolostone has a Young's modulus of

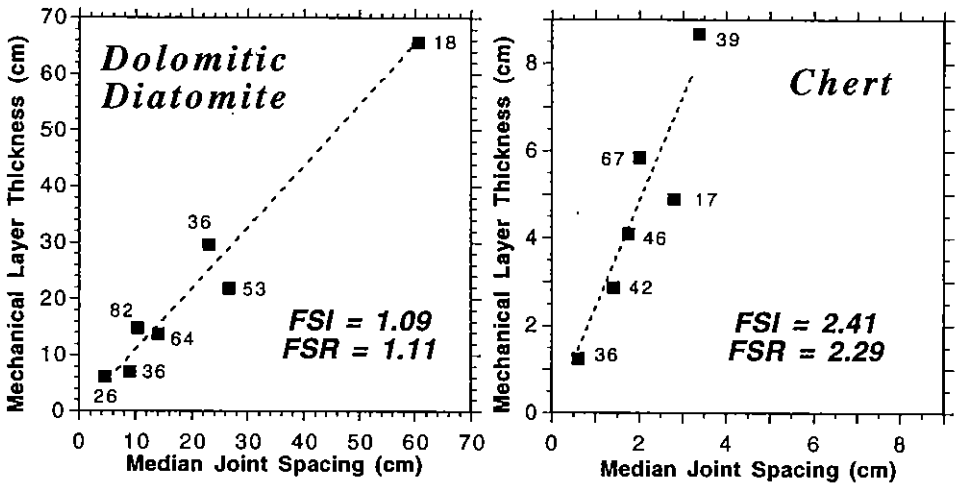

Fig. 13. Median joint spacing v. mechanical layer thickness for diatomite and chert beds of the Monterey Formation exposed at Lompoc Landing. Numbers next to data points refer to total number of joint spacing measurements taken in that particular bed.

56 GPa and a K_{Ic} of 1.7 MPa $m^{1/2}$, whereas the sandstone has a Young's modulus of 12 GPa and a K_{Ic} of 1.2 MPa $m^{1/2}$. Hooke's Law states that for a given value of strain, stress will be higher in the bed with the higher Young's modulus (Fig. 14). Because our fracture criterion is a threshold stress value (i.e. the fracture stress, σ_f), jointing will occur in a given bed at the point where the stress–strain curve intersects σ_f for that bed. Assuming a range in flaw size from 0.3 to 0.5 cm (i.e. crack half-lengths of 0.15–0.25 cm) for both jointing lithologies, the fracture stress is 19.2–24.8 MPa for the dolostone and 13.5–17.5 MPa for the sandstone (Fig. 14).

Fracture stress ranges derived from the range in flaw size correspond in turn to a range of strain values for the first jointing event in each lithology. The intersections of stress–strain curves with horizontal fracture stress lines in Fig. 14 indicate that joints will propagate in the dolostone bed for strain values within the range of 3.43×10^{-4} to 4.42×10^{-4}. Likewise, joints will initiate in the sandstone unit between strains of 1.12×10^{-3} and 1.46×10^{-3}. In the case whereby all beds in the rock mass are welded together, and thus remote longitudinal strain remains uniform throughout, the first series of joints will propagate in the dolostone bed once a strain of *c.* 4×10^{-4} is reached. At this juncture the sandstone bed is unjointed because stress within the sandstone is less than the minimum fracture stress of 13.5 MPa. As longitudinal extension continues, the sandstone bed remains unjointed until strain values of 1.12×10^{-3}–1.46×10^{-3} are exceeded, at which point the first set of joints propagates in the sandstone.

As a result of the relationship between Hooke's Law and the fracture stress criterion, jointing occurs in the dolostone at lower strains, and hence earlier, than jointing in the sandstone. In fact, the situation may arise where a stiff bed undergoes two or more jointing events prior to initial jointing in a low modulus bed. Therefore, in spite of the larger stress reduction shadows predicted by both Hobbs and finite element modelling, beds with relatively high Young's moduli can actually contain relatively closely-spaced joints by virtue of the small strain increments required for infilling jointing events.

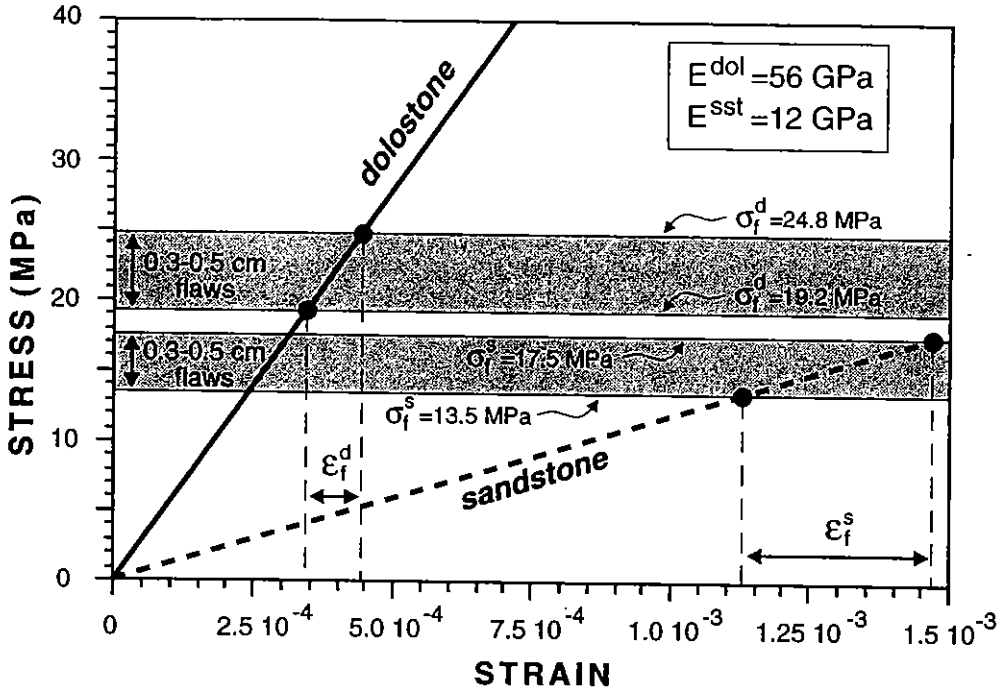

Fig. 14. Fracture stress ranges superimposed on stress–strain plots for typical dolostone and sandstone beds. Ranges in fracture stress correspond to a range in flaw size from 0.3 to 0.5 cm. Note the dolostone bed will fracture at lower strain levels than the sandstone. See text for details.

In comparing two jointing beds with different elastic moduli (for Beds 1 and 2, $E_1 > E_2$), the factor that determines which bed will fracture at lower strains is the ratio of Young's modulus to the ratio of fracture stress. Assuming the same range of flaw sizes for both beds, the stiffer bed will fracture at lower strains when:

$$\frac{E_1}{E_2} > \frac{K_{Ic}^{(1)}}{K_{Ic}^{(2)}}. \tag{7}$$

The inequality in equation (7) holds true for a majority of sedimentary rocks, which may explain the higher joint densities often observed in stiffer beds despite the larger stress reduction shadows.

Conclusions

Joint spacing models focus on the distribution of tensile stress about a joint in an effort to predict the location of subsequent joints. Stress distributions derived from finite element simulations compare favourably with Hobbs' theoretical predictions. Both the Hobbs model and finite element modelling predict longer stress reduction shadows, and hence wider joint spacings, for beds with higher Young's moduli. Finite element simulations,

though, show the dependence of the stress reduction shadow on Young's modulus in the jointing bed is weaker than the square root dependence predicted by Hobbs.

Though bed thickness is a primary factor, elastic moduli, extensional strain and flaw size are all important parameters determining joint spacing in interbedded sedimentary rocks. A high Young's modulus contributes to an increase in stress reduction shadow length, yet tends to lower the strain level required for joint propagation due to its relationship with the fracture stress criterion. Small flaws situated in the middle of the jointing bed produce widely spaced joints, whereas those same flaws located near bed interfaces result in more closely spaced joints. Despite the complex interaction among these factors, creating a wide range of joint spacings for an individual mechanical bed, the linear correlation between median joint spacing and bed thickness for a given lithology, and hence given mechanical properties, is remarkably strong.

Funding for this project was provided by a grant from Texaco (TE, MRG) a Shell Doctoral Fellowship (MPF) and GRI Contract 5088-260-1746 (TE). We thank T. Ingraffea for providing the finite element program, T. Bittencourt and D. Swenson for technical assistance and Wendy Bartlett for helpful field information. We appreciate the thoughtful reviews provided by Wayne Narr, Atilla Aydin, Byron Kulander, Ernie Rutter and Mohammed Ameen.

References

ATKINSON, B. K. & MEREDITH, P. G. 1987. Experimental fracture mechanics data for rocks and minerals. *In:* ATKINSON, B. K. (ed.) *Fracture Mechanics of Rock*. Academic Press, London, 477–525.

BARSOUM, R. S. 1976. On the use of isoparametric finite elements in linear fracture mechanics. *International Journal of Numerical Methods in Engineering*, **10**, 25–37.

BLAIR, B. E. 1955. *Physical properties of mine rock, Part 3*. US Bureau of Mines Report of Investigations 5130.

——— 1956. *Physical properties of mine rock, Part 4*. US Bureau of Mines Report of Investigations 5244.

BROEK, D. 1978. *Elementary Engineering Fracture Mechanics*. Sijthoff & Noordhoff, Dordrecht, the Netherlands.

CLARK, S. P. 1966. *Handbook of Physical Constants*. Geological Society of America Memoir, **97**.

COX, H. L. 1952. The elasticity and strength of paper and other fibrous materials. *British Journal of Applied Physics*, **3**, 72–79.

DAVIDGE, R. W. 1979. *Mechanical Behavior of Ceramics*. Cambridge University Press, Cambridge, UK.

ENGELDER, T. & GROSS, M. R. 1993. Curving cross joints and the lithospheric stress field in eastern North America. *Geology*, **21**, 817–820.

FISCHER, M. P. 1994. *Application of linear elastic fracture mechanics to some problems of fracture propagation in rock and ice*. PhD Thesis, Pennsylvania State University, USA.

GARRETT, K. W. & BAILEY, J. E. 1977. Multiple transverse fracture in 90° cross-ply laminates of a glass fibre-reinforced polyester. *Journal of Materials Science*, **12**, 157–168.

GRIFFITH, A. A. 1920. The phenomena of rupture and flow in solids. *Philosophical Transactions of the Royal Society of London*, **A221**, 63–197.

GROSS, M. R. 1993*a*. The origin and spacing of cross joints. *Journal of Structural Geology*, **15**, 737–751.

——— 1993*b*. *The effects of mechanical stratigraphy on failure mode and fracture spacing in the Monterey Formation of coastal California*. PhD Thesis, Pennsylvania State University, USA.

HOBBS, D. W. 1967. The formation of tension joints in sedimentary rocks: an explanation. *Geological Magazine*, **104**, 550–556.

HUANG, Q. & ANGELIER, J. 1989. Fracture spacing and its relation to bed thickness. *Geological Magazine*, **126**, 355–362.

INGLIS, C. E. 1913. Stresses in a plate due to the presence of cracks and sharp corners. *Transactions of the Institute of Naval Architecture*, **55**, 219–230.

IRWIN, G. R. 1957. Analysis of stresses and strains near the end of a crack traversing a plate. *Journal of Applied Mechanics*, **24**, 361–364.

JAEGER, J. C. & COOK, N. G. W. 1976. *Fundamentals of Rock Mechanics*. Chapman & Hall, London.

LACHENBRUCH, A. H. 1961. Depth and spacing of tension cracks. *Journal of Geophysical Research*, **66**, 4273–4292.

LADEIRA, F. L. & PRICE, N. J. 1981. Relationship between fracture spacing and bed thickness. *Journal of Structural Geology*, **3**, 179–183.

LAWN, B. R. & WILSHAW, T. R. 1975. *Fracture of Brittle Solids*. Cambridge University Press, Cambridge, UK.

MASUDA, T. & KURIYAMA, M. 1988. Successive 'mid-point' fracturing during microboudinage: an estimae of the stress–strain relation during a natural deformation. *Tectonophysics*, **147**, 171–177.

MCQUILLAN, H. 1973. Small-scale fracture density in Asmari Formation of southwest Iran and its relation to bed thickness and structural setting. *American Association of Petroleum Geologists Bulletin*, **57**, 2367–2385.

NARR, W. & SUPPE, J. 1991. Joint spacing in sedimentary rocks. *Journal of Structural Geology*, **13**, 1037–1048.

OLSON, J. & POLLARD, D. D. 1989. Inferring paleostresses from natural fracture patterns: A new method. *Geology*, **17**, 345–348.

PARIS, P. C. & SIH, G. C. 1965. *Stress Analysis of Cracks*. American Society of Testing and Materials, Special Publication, **381**, 30–76.

PARVIZI, A. & BAILEY, J. E. 1978. On multiple transverse cracking in glass fibre epoxy cross-ply laminates. *Journal of Materials Science*, **13**, 2131–2136.

POLLARD, D. D. & SEGALL, P. 1987. Theoretical displacements and stresses near fracture in rock: with applications to faults, joints, veins, dikes, and solution surfaces. *In:* ATKINSON, B. K. (ed.) *Fracture Mechanics of Rock*. Academic Press, London, 277–349.

———, SEGALL, P. & DELANEY, P. T. 1982. Formation and interpretation of dilatant echelon cracks. *Geological Society of America Bulletin*, **93**, 1291–1303.

PRICE, N. J. 1966. *Fault and Joint Development in Brittle and Semi-brittle Rocks*. Pergamon Press, Oxford.

PRIEST, D. S. & HUDSON, J. A. 1976. Discontinuity spacings in rock. *International Journal of Rock Mechanics, Mining Sciences, and Geomechanics Abstracts*, **13**, 135–148.

RIVES, T., RAZACK, M., PETIT, J.-P. & RAWNSLEY, K. D. 1992. Joint spacing: analogue and numerical simulations. *Journal of Structural Geology*, **14**, 925–937.

ROULEAU, A. & GALE, J. E. 1985. Statistical characterization of the fracture system in the Stripa Granite, Sweden. *International Journal of Rock Mechanics, Mining Sciences, and Geomechanics Abstracts*, **22**, 353–367.

SENSENY, P. E. & PFEIFLE, T. W. 1984. Fracture toughness of sandstones and shales. *Proceedings of the 25th US Symposium on Rock Mechanics*. Society of Mining Engineers of the American Institute of Mining, Metallurgical and Petroleum Engineers, Inc., New York, 390–397.

SYLVESTER, A. G. & DARROW, A. C. 1979. Structure and neotectonics of the western Santa Ynez fault system in southern California. *Tectonophysics*, **52**, 389–405.

WAWRZYNEK, P. A. & INGRAFFEA, A. R. 1987. Interactive finite element analysis of fracture processes: an integrated approach. *Theoretical and Applied Fracture Mechanics*, **8**, 137–150.

WEIBULL, W. 1951. A statistical distribution function of wide applicability. *Journal of Applied Mechanics*, **18**, 293–297.